Magnetically Induced Anisotropic Orientation of Graphene Oxide Locked by *in Situ* Hydrogelation

Linlin Wu,[†,∥] Masataka Ohtani,[‡,∥] Masaki Takata,[§] Akinori Saeki,[⊥] Shu Seki,[⊥] Yasuhiro Ishida,[‡,*] and Takuzo Aida[†,‡]

[†]Department of Chemistry and Biotechnology, School of Engineering, The University of Tokyo, 7-3-1 Hongo, Bunkyo, Tokyo 113-8656, Japan, [‡]RIKEN Center for Emergent Matter Science, 2-1 Hirosawa, Wako, Saitama 351-0198, Japan, [§]RIKEN SPring-8 Center, 1-1-1 Kouto, Sayo, Hyogo 679-5198, Japan, and [⊥]Department of Applied Chemistry, Osaka University, 2-1 Yamadaoka, Suita, Osaka 565-0871, Japan. [∥]L. Wu and M. Ohtani contributed equally to this work.

ABSTRACT A general method to prepare polymer gels containing anisotropically oriented graphene oxide (GO) or reduced graphene oxide (RGO) was developed, by using the magnetically induced orientation of GO. Under a magnetic field, an aqueous dispersion of GO was gelated by *in situ* cross-linking polymerization of an acryl monomer and a cross-linker. In the resultant hydrogel, the orientation of GO was retained even in the absence of the magnetic field, because the gel network trapped GO *via* noncovalent interactions and efficiently suppressed the structural relaxation of GO. The locked structure enabled quantitative investigation on the magnetic orientation of GO using 2D small-angle X-ray scattering, which revealed that GO nanosheets orient parallel to the magnetic field with an order parameter of up to 0.80. Systematic studies with varying gelation conditions indicate that the present method can afford a wide range of GO-hybridized anisotropic materials, in terms of GO alignment direction, sample shape, and GO concentration. Also by virtue of the locked structure, the orientation of GO in the hydrogel was well preserved throughout the *in situ* chemical reduction of GO, yielding an RGO-hybridized anisotropic hydrogel, as well as the conversion of the hydrogel into organo- and ionogels through the replacement of the internal water with solvents. As a preliminary demonstration of the present method for practical application, a polymer-composite film containing RGO oriented vertical to the film surface was prepared, and its anisotropically enhanced electroconductivity along the orientation direction of RGO was confirmed by the flash-photolysis time-resolved microwave conductivity measurement.

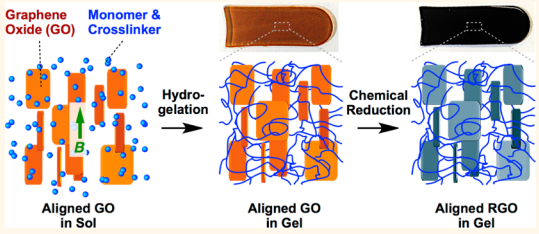

KEYWORDS: anisotropy · hydrogels · graphene oxide · graphene · magnetic field

The rapid progress made in nanosciences had led to the availability of 2D nanosheets with various structures and functions.[1−5] Among them, graphene oxide (GO), the oxygenated form of a monolayer graphene platelet that can be exfoliated in polar media, has recently attracted considerable attention.[6−14] Due to its solution processability and chemical modifiability, GO serves as a precursor for various carbon-based composite materials. Particularly, GO is readily converted into its reduced form (reduced graphene oxide, RGO), allowing for enhancement in the electrical properties of the nanosheets.[7,11,15−18] Not only as a precursor of RGO, GO can also be used as a nanofiller to reinforce and functionalize composite materials[19−23] owing to its high mechanical properties, extremely large surface area, and abundance of polar functionalities on its surface.

For the creation of novel composite materials hybridized with 2D nanosheets, the anisotropic orientation of nanosheets over a macroscopic size scale is an attractive challenge.[24−30] Such composite materials often show unique anisotropic features in mechanical toughness,[24,26,28,30] optical properties,[28] and thermal/electrical/ion conductivities.[25,27,29] For the anisotropic orientation of GO, a layer-by-layer assembly using the Langmuir−Blodgett technique[31,32] and vacuum filtration-assisted self-assembly[7,33−38] have been widely used. However, these conventional methods have a number of limitations such as lengthy process, low scalability, poor tunability of GO direction/GO concentration, and difficulty in obtaining bulk (nonfilm) materials. Indeed, these methods can afford only film-shaped materials with densely stacked, in-plane-oriented GO nanosheets. More recently, GOs

* Address correspondence to y-ishida@riken.jp.

Received for review January 21, 2014 and accepted April 16, 2014.

Published online April 16, 2014
10.1021/nn5003908

coated with paramagnetic particles have been developed.[39] Although such modified GOs can be readily aligned using a magnetic field, the resultant materials are inevitably contaminated with paramagnetic species, which severely limits their application.

To develop a more general methodology for the preparation of anisotropic GO/RGO-hybridized materials, we focused on the fact that strong magnetic fields can align anisotropically shaped diamagnetic nanostructures, such as inorganic nanosheets[40] and platelets,[41] lipid bilayers,[42] organic nanocrystals,[43] and proteins.[44] Although magnetic susceptibility of diamagnetic species is generally low, aromatic molecules often show exceptionally large diamagnetic susceptibility in the orthogonal direction to their planes, because of the diamagnetic "ring-current" effect of their π-conjugated systems. Therefore, aromatic molecules tend to orient their planes parallel to the magnetic field.[45] Particularly in the case of carbon nanoclusters composed of large numbers of ordered aromatic rings, such as carbon nanotubes, graphene, GO, and RGO, their magnetic orientation energy can overcome thermal fluctuation.[46] Unlike other external stimuli (shear force, flow, gravity, electric field, *etc.*), magnetic field can be applied in a nondestructive and contactless manner without any limitation in size and shape of samples and, therefore, is quite attractive. However, there has been only one report regarding the magnetic orientation of GO devoid of paramagnetic particles, wherein the macroscopic orientation of GO in aqueous dispersions was confirmed by polarized optical microscopy.[47] Thus, the quantitative characterization and further applications of magnetically oriented GO have hardly been reported hitherto, most likely because such magnetically oriented materials are not useful for analysis and fabrication. Due to the low magnetic susceptibility and easy thermal fluctuation of GO nanosheets dispersed in fluids, a relatively strong magnetic field (>~0.25 T) should be continuously applied to maintain a satisfactorily ordered structure.

With the objective of overcoming such limitations, we report herein a conceptually novel approach to investigate and fabricate magnetically oriented GO in aqueous dispersions by locking the ordered structure using *in situ* hydrogelation (Scheme 1).[30,42,48−51] By taking advantage of the benefits of magnetic treatment, as described above, GO could be oriented without any limitation in orientational direction and sample shape. In the resultant hydrogels, the structural order of GO was preserved in the absence of the magnetic field, thereby allowing for a detailed analysis of the structure of oriented GO using 2D small-angle X-ray scattering (2D SAXS). Owing to the excellent stability of the gel network, the ordered structures of GO nanosheets were well preserved even after treatment with chemicals, affording various GO-hybridized composite gels with macroscopic anisotropy. In particular,

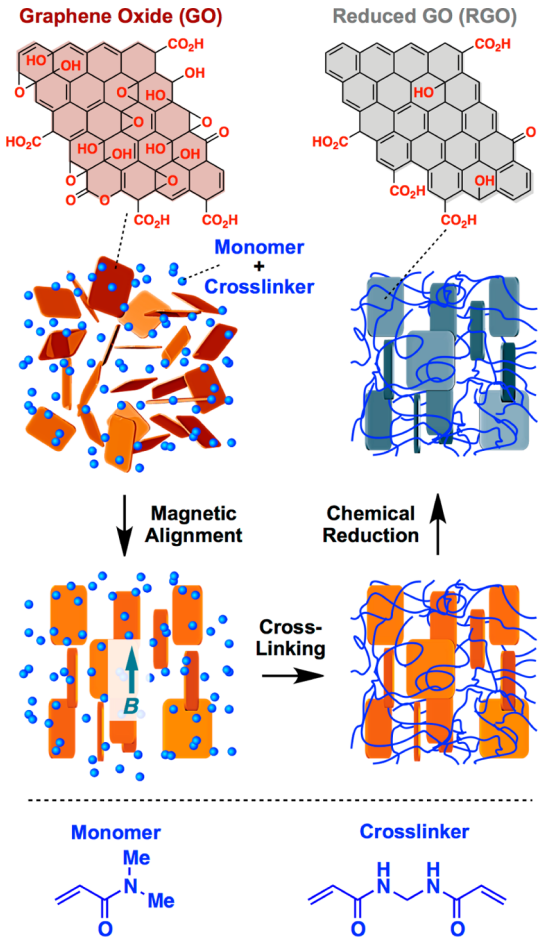

Scheme 1. Preparation of composite gels with macroscopically oriented GO/RGO *via* cross-linking polymerization of acrylamide derivatives in a magnetic field and subsequent chemical reduction of GO.

the *in situ* reduction of GO nanosheets readily proceeded to yield composite gels containing macroscopically oriented RGO nanosheets (Scheme 1).

RESULTS AND DISCUSSION

Preparation and Characterization of the Anisotropic GO-Hybridized Hydrogel. An aqueous dispersion of GO (average size = ~50 μm, [GO] = 0.2 wt %)[52,53] was converted into an anisotropic GO-hybridized hydrogel by *in situ* cross-linking polymerization of an acryl monomer (*N*,*N*-dimethylacrylamide, 3.0 wt %) and a cross-linker (*N*,*N*′-methylenebis(acrylamide), 0.16 wt %) in a 10 T magnetic field (see Experimental Methods). The cross-linking polymerization proceeded almost quantitatively to yield a brown, transparent, and free-standing hydrogel (Figure 1a). As confirmed by polarized optical microscopy (POM), GO nanosheets were unidirectionally oriented over an entire region of the resultant hydrogel. The POM image of the hydrogel (1 mm thick) under crossed polarizers showed a contrast at every 45° on rotation, giving a completely dark image when the azimuthal angle between the polarized direction of the incident light and the magnetic

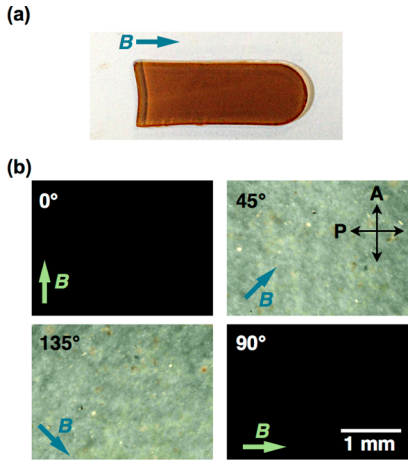

Figure 1. (a) Picture of a GO-hybridized hydrogel (~50 μm-sized GO/monomer/cross-linker = 0.20/3.0/0.16 wt %, 1 mm thick, prepared in a 10 T magnetic field). (b) POM images of the GO-hybridized hydrogel (1 mm thick) obtained by varying the angle between the direction of the analyzer and that of the applied magnetic field (0°, 45°, 90°, and 135°). *B*: magnetic field.

flux line was either 0° or 90° (Figure 1b). This indicates that the GO nanosheets oriented either parallel or orthogonal to the applied magnetic field. The same trend was observed at arbitrarily selected viewing fields in the hydrogel, proving that the domain containing oriented GO was developed over the entire sample. The SEM/EDS measurements of the GO powder at the start suggested that the amount of the contaminated paramagnetic species was negligibly small, excluding the effect of the paramagnetic impurities on the present magnetic orientation (Figure S4).

For the quantitative evaluation of the orientation of GO, 2D SAXS analysis was performed (Figure 2). Upon exposure to an X-ray beam orthogonal to the applied magnetic field, the GO-hybridized hydrogel (~50 μm-sized GO/monomer/cross-linker = 0.20/3.0/0.16 wt %), prepared in a 10 T magnetic field, exhibited an elliptical diffusive pattern that oriented its longer axis orthogonal to the direction of the magnetic field (Figure 2a). Meanwhile, when exposed to an X-ray beam parallel to the magnetic field, the hydrogel yielded an isotropic scattering (Figure 2b). This scattering supposedly did not originate from the polymer matrix but rather from GO nanosheets because the scattering of the GO-free hydrogel matrix was negligibly weak (Figure S8a). In principle, 2D nanosheets can take a parallel or orthogonal orientation to the applied field, and the present data unambiguously proved that the GO planes in the hydrogel oriented parallel to the magnetic field,[54] similar to previous reports on the magnetic alignment of 2D nanosheets.[40−43] Accordingly, the azimuthal angle (φ) plot of the 2D SAXS pattern measured from the orthogonal direction to the magnetic field has two peaks, at $\theta = 90°$ and 270° (Figure 2c, red), whereas the measurement parallel to the magnetic field shows a single plateau (Figure 2c, blue). On the basis of

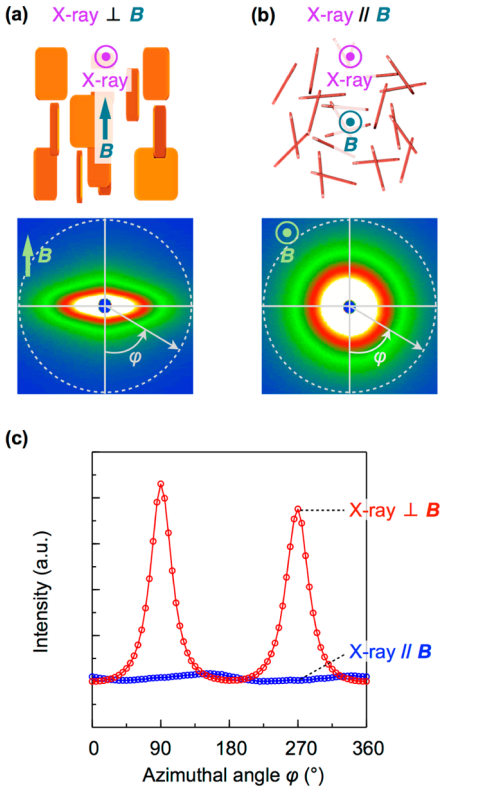

Figure 2. (a, b) 2D SAXS images of a GO-hybridized hydrogel (~50 μm-sized GO/monomer/cross-linker = 0.20/3.0/0.16 wt %, prepared in a 10 T magnetic field). The hydrogel was exposed to an X-ray beam from the orthogonal (a) and parallel (b) directions to the applied magnetic field. (c) Azimuthal angle (φ) plots for the 2D SAXS images in (a) and (b).

the fitting of the azimuthal angle plot for Figure 2a (Figure 2c, red) to a Maier−Saupe distribution function, the orientation order parameter was estimated to be 0.80,[54,55] which is relatively high compared with other magnetically oriented 2D nanosheets.[40−42] Noteworthy, the orientation of GO was hardly influenced by the direction of gravity (Figure S5) and sample shape (Figure S6), which is one of the most prominent features of the present method compared to the conventional GO orientation methods.[7,31−39]

In the anisotropic GO-hybridized hydrogels, the alignment of GO nanosheets was preserved after the magnetic field was removed or even when the hydrogel was placed in magnetic fields that were not parallel to the orientation direction of GO nanosheets (Figure S10), indicating that the GO nanosheets strongly interacted with gel networks composed of acryl polymer chains so that their structural relaxation was efficiently suppressed. Such strong interactions between the GO nanosheets and gel networks were also implied by the unique mechanical properties of the GO-hybridized hydrogels, wherein the GO served as a nanofiller to reinforce the hydrogel in an anisotropic manner. As shown in Figure 3, elastic moduli (G') of the GO-hybridized hydrogel (blue and red circles, G' = 1200−2300 Pa) were 20−40 times

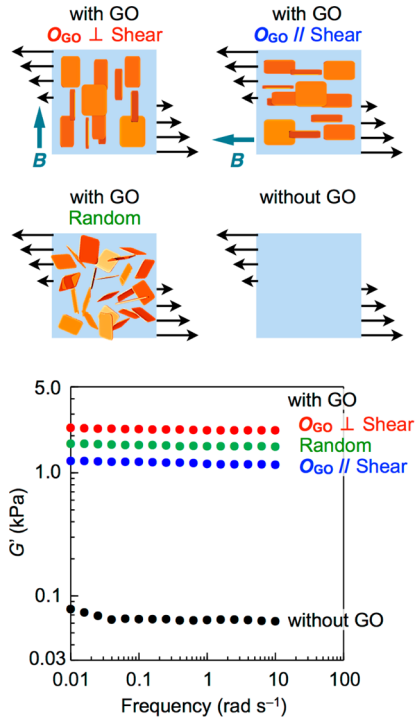

Figure 3. Rheological properties of an anisotropic GO-hybridized hydrogel (~50 μm-sized GO/monomer/cross-linker = 0.20/3.0/0.16 wt %) prepared in a 10 T magnetic field sheared in the directions orthogonal (red circles) and parallel (blue circles) to the orientation vector of GO nanosheets), an analogous hydrogel prepared without magnet (green circles), and a GO-free hydrogel (monomer/cross-linker = 3.0/0.16 wt %; black circles). Storage moduli (G') on frequency sweep (0.01−10 rad s^{-1}) at a fixed strain (0.5%). O_{GO}: orientation vector of GO nanosheets.

greater than that of a GO-free hydrogel (monomer/cross-linker = 3.0/0.16 wt %, black circles; G' = 65 Pa). In addition, between the G' values for shear orthogonal (red circles) and parallel (blue circles) to the orientation vector of GO nanosheets, the GO-hybridized hydrogel showed a nonnegligible difference (2300 and 1200 Pa, respectively). An analogous hydrogel with randomly oriented GO nanosheets, prepared without magnet, showed G' values (green circles) at an intermediate level between those of the anisotropic GO-hybridized hydrogel measured in the directions parallel and orthogonal to the orientation vector of the GO nanosheets. These observations clearly indicate that the mechanical anisotropy of the hydrogel originates from the anisotropic alignment of GO nanosheets. Such an efficient (20−40 times enhancement by 0.20 wt % doping) and anisotropic reinforcement implies strong interaction between GO nanosheets and the gel network. In relation to this, we also measured SEM images of the xerogel of the anisotropic GO-hybridized hydrogel and found that polymeric fibers were oriented parallel to the applied magnetic field (Figure S11).

Scope and Limitation of Magnetic GO Orientation. To clarify the scope and limitation of the present method for the orientation of GO nanosheets, the effects of the parameters (magnetic field intensity, GO concentration, and GO size) on the orientation order parameters, which can be unambiguously estimated based on 2D SAXS as shown in Figure 2, were systematically investigated (Figure 4 and Figures S7−S9).

To investigate the effect of magnetic-field intensity, four kinds of GO-hybridized hydrogels (~50 μm-sized GO/monomer/cross-linker = 0.20/3.0/0.16 wt %) were prepared using the aforementioned procedure and varying the intensity of the applied magnetic field (0, 1, 5, and 10 T). Upon decreasing the field intensity from 10 T to 5 T, the orientation order parameter hardly changed (from 0.80 to 0.78; Figure 4a and d, red and blue). However, a further decrease in the magnetic-field intensity caused a significant drop in the orientation order parameter (Figure 4a and d, green). Thus, ~5 T was found to be the critical intensity to realize the maximum degree of orientation.

Next, the effect of GO concentration was studied using hydrogels with different GO content (0.02, 0.05, 0.10, and 0.20 wt %), which were prepared using the aforementioned procedure (monomer/cross-linker = 3.0/0.16 wt %) in a 10 T magnetic field. The 2D SAXS studies of these hydrogels indicate that the orientation order parameter was well retained through dilution (Figure 4e); upon decreasing GO concentration from 0.20 to 0.02 wt %, the half-widths of the two peaks in the azimuthal angle plot were essentially unchanged, although their heights became smaller in proportion to GO concentration (Figure 4b). This clearly proves that the present method can afford highly oriented composite materials even at an extremely low GO concentration, unlike other conventional methods used for GO orientation.

In the above investigations, GO nanosheets with relatively large size (~50 μm) were employed. To clarify the scope and limitation of the magnetic orientation method in terms of GO size, another GO sample with smaller average size (~0.3 μm) was prepared from a graphite source with an average size of 45 μm (Figures S1−S4). By using an aqueous dispersion of the smaller GO, we prepared a hydrogel (~0.3 μm-sized GO/monomer/cross-linker = 0.10/3.0/0.16 wt %) in a 10 T magnetic field using the same procedure. 2D SAXS measurement revealed that the smaller GO attained only a moderate level of orientation with an order parameter of ~0.4 (Figure 4c and f, blue). Such a drastic effect of GO size on the degree of orientation is elucidated as follows. First, the increment of GO size is accompanied by the reduction of thermal fluctuation and enhancement of shape anisotropy, both of which yield a favorable effect on the magnetic orientation of GO.[30] In addition, GO size is known to be a crucial factor for the liquid crystalline behavior of its aqueous dispersions,[47,57,58] which is also anticipated to impact the orientability of GO. Indeed, upon reducing the GO concentration from 0.20 wt % to 0.01 wt %, the aqueous dispersions of the larger GO (average size = ~50 μm)

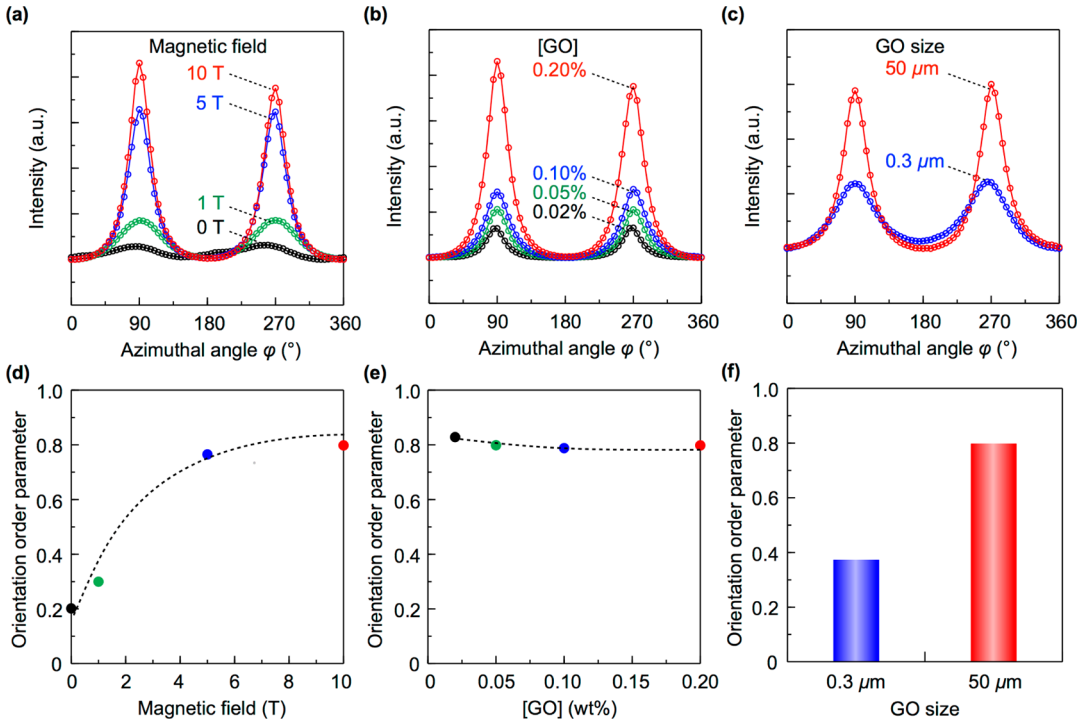

Figure 4. (a–c) Azimuthal angle plots for 2D SAXS images (X-ray ⊥ *B*) of GO-hybridized hydrogels (GO/monomer/cross-linker = 0–0.20/3.0/0.16 wt %) prepared by varying magnetic-field intensity (a), GO concentration (b), and GO size (c). (d–f) Plots of the orientation order parameter of GO nanosheets to magnetic-field intensity (d), GO concentration (e), and GO size (f).

always exhibited a nematic phase, whereas those of the smaller GO (averaged size = ~0.3 μm) were isotropic (Figure S12).

Through the above studies, optimal conditions were established for the preparation of GO-hybridized hydrogels with a high degree of GO orientation. In the following sections, the GO-hybridized hydrogel (~50 μm-sized GO/monomer/cross-linker = 0.20/3.0/0.16 wt %, prepared in a 10 T magnetic field), exhibiting the highest orientation order parameter of 0.80, was employed.

***In Situ* Chemical Reduction of GO to RGO in the Anisotropic Hydrogel.** With anisotropic GO-hybridized hydrogels in hand, we next attempted to convert GO in the hydrogels into reduced GO, in order to enhance its electrical properties.[15−18] Since harsh conditions are not suitable for our hydrogel-based materials, we chose a chemical reduction method that was recently reported.[59,60] For example, the anisotropic GO-hybridized hydrogel was successively treated with aqueous solutions of KOH (1.6 M) and HI (55%). As a result, the brown-colored gel turned black (Figure 5a and b, top), suggesting that the graphitic domains in the nanosheets were increased by the reduction of the defects of oxygen-containing functionalities. To estimate the reduction degree of RGO, X-ray photoelectron spectroscopy (XPS) of the xerogel of the resultant hydrogel was performed (Figure 5a and b, bottom). Although the polymer network contained C═O groups and therefore this measurement inevitably suffered from background signals,

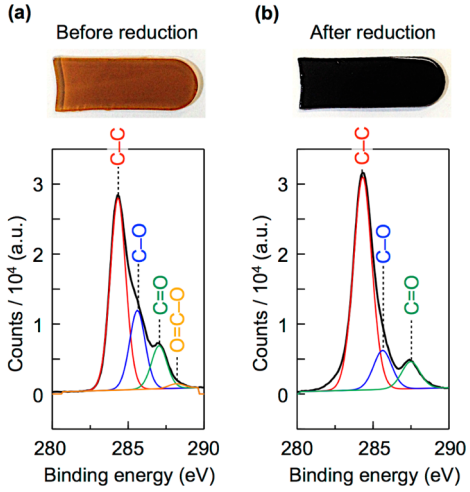

Figure 5. Pictures (1 mm thick, top) and XPS spectra (bottom) of GO/RGO-hybridized hydrogels. (a) GO-hybridized hydrogel (~50 μm-sized GO/monomer/cross-linker = 0.20/3.0/0.16 wt %, prepared in a 10 T magnetic field). (b) RGO-hybridized hydrogel obtained by the chemical reduction of GO in the GO-hybridized hydrogel.

the integrated intensity of the three peaks with binding energies of 285.6, 287.0, and 288.3 eV, attributed to C–O, C═O, and O═C–O, respectively, was decreased from 49% to 34% through the reduction.[61] Furthermore, a model reaction was performed by using an aqueous GO dispersion ([GO] = 0.20 wt %), in place of the GO-hybridized hydrogel ([GO] = 0.20 wt %), where carbon clusters (GO and RGO) could be quantitatively recovered from the reaction mixture. In the elemental

analysis of the recovered carbon clusters, the oxygen content was decreased from 37% to 23%. These observations suggest that the reduction of GO in the present hydrogel proceeded at a satisfactory level.

Interestingly, the ordered structure of GO was well preserved throughout the reduction, wherein the orientation order parameter, estimated from the azimuthal angle plot of the 2D SAXS image (Figure 6a and Figure S13), decreased from 0.80 to 0.76 (Figure 6b). As in the case of the precursor GO-hybridized hydrogels, the RGO-oriented domain developed over the entire sample, as confirmed using POM (Figure S14). Such a homogeneous and anisotropically structured RGO-hybridized hydrogel could not be obtained by a "prereduction" approach. Thus, when an aqueous dispersion of GO was treated with the reducing agents, the system immediately started to generate precipitates of RGO (Figure S15a). Although samples of RGO with relatively small sizes are processable in solution,[7,61] those with *ca.* micrometer sizes, as we used in this work, are hardly dispersible in aqueous media and exist as aggregates of randomly oriented RGO nanosheets. Therefore, when the resultant mixture was subjected to the *in situ* hydrogelation under a 10 T magnetic field in the same manner as the preparation of anisotropic GO-hybridized hydrogels, a hydrogel containing heavily stacked RGO sheets with essentially no anisotropic orientation was afforded (Figure S15b).

Conversion of the Anisotropic RGO-Hybridized Hydrogel into Organo- and Ionogels. Importantly for practical applications, the anisotropic orientation of RGO was well preserved even when the internal water of the hydrogel was replaced with other fluids, owing to the stable gel network. For example, the RGO-hybridized hydrogel, prepared by the chemical reduction of GO in the GO-hybridized hydrogel, was immersed in ethanol (EtOH) at 20 °C for 12 h three times in a fresh solvent (1000 vol %), wherein internal water was replaced with EtOH to afford a homogeneous, tough material (Figure 7a).

It is worth noting that the thorough replacement of internal fluids brought only slight deterioration in the orientational order of RGO, as confirmed by 2D SAXS studies (Figure 7b and c and Figure S16). As shown in Figure 7b and c (blue), the orientation order parameter of the resultant gel was comparable to that of the original hydrogel. Not only EtOH but also other solvents such as ethylene glycol (EG) and an ionic liquid (1-butyl-4-methylimidazolium tetrafluoroborate, $BMImBF_4$) could replace the gelling water, affording tough organogels and ionogels, although a rather remarkable volume contraction took place in the case of the ionogel (Figure 7a). Again, the resultant material retained the anisotropically oriented structure of RGO (Figure 7b and c, green and black). Needless to say, the GO-hybridized hydrogel could also be converted into organo- and ionogels without a drastic decrease in anisotropy (Figure S17), under the conditions otherwise

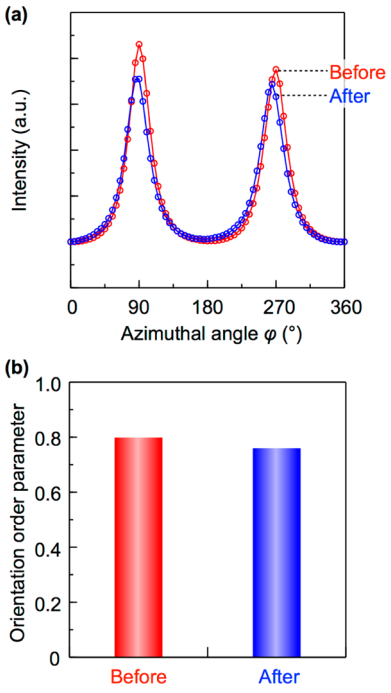

Figure 6. (a, b) Azimuthal angle plots for 2D SAXS images (X-ray ⊥ *B*) (a) and orientation order parameters (b) of GO/RGO-hybridized hydrogels. Red: GO-hybridized hydrogel (~50 μm-sized GO/monomer/cross-linker = 0.20/3.0/0.16 wt %, prepared in a 10 T magnetic field). Blue: RGO-hybridized hydrogel obtained by the chemical reduction of GO in the GO-hybridized hydrogel.

identical to those used for the GO-hybridized hydrogels. Considering the limited volatility of EG and $BMImBF_4$, the organogels and ionogels hybridized with macroscopically oriented GO/RGO would have multiple applications.

Anisotropic Electroconductivity of the RGO-Hybridized Gel. As described in the introductory part, RGO−polymer composites have attracted increasing attention as electroconductive soft materials. In particular, the vacuum filtration-assisted self-assembly of RGO is known to yield film-shaped materials with densely stacked, in-plane-oriented RGO nanosheets, which show anisotropically enhanced electroconductivity along the film-surface direction.[33] Meanwhile, for RGO-hybridized films with vertically oriented RGO nanosheets, only a few examples have been reported,[39,62,63] and the preparation of such films by a generalizable methodology still remains an attractive challenge. Since the present method can control the orientation direction of RGO nanosheets without any limitation in sample shape, a film-shaped RGO-hybridized hydrogel (~1 mm thick) containing vertically oriented RGO nanosheets could be successfully prepared by the aforementioned method, *i.e.*, the chemical reduction of GO in a GO-hybridized hydrogel film (~50 μm-sized GO/monomer/cross-linker = 0.20/3.0/0.16 wt %) prepared in a 10 T magnetic field that was directed orthogonal to the film surface.

To demonstrate the potential utility of this film, we attempted to evaluate the anisotropy in its

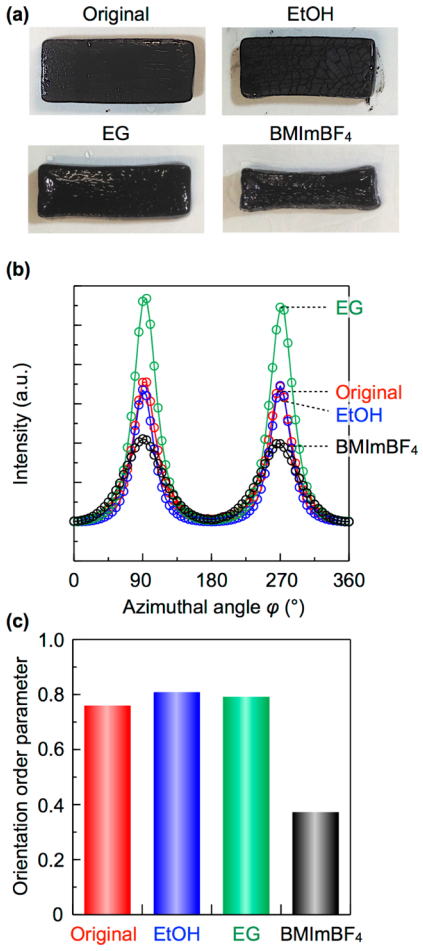

Figure 7. (a) Pictures (5 mm thick), (b) azimuthal angle plots for 2D SAXS images (X-ray ⊥ *B*), and (c) orientation order parameters of RGO-hybridized hydro-, organo-, and ionogels. An RGO-hybridized hydrogel, prepared by the chemical reduction of GO in a GO-hybridized hydrogel (~50 μm-sized GO/monomer/cross-linker = 0.20/3.0/0.16 wt %, prepared in a 10 T magnetic field), was immersed in ethanol (EtOH), ethylene glycol (EG), or 1-butyl-4-methylimidazolium tetrafluoroborate ($BMImBF_4$) at 20 °C for 12 h three times in a fresh solvent (1000 vol %).

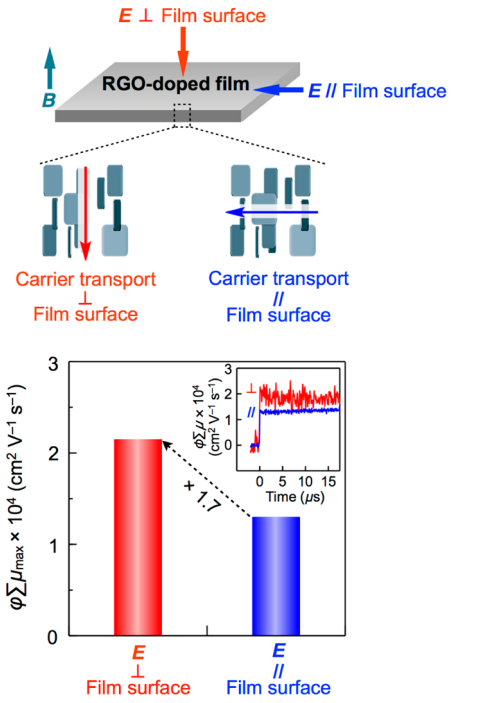

Figure 8. Maximum transient conductivities ($\varphi\Sigma\mu$: φ = photocarrier generation yield, $\Sigma\mu$ = sum of the mobilities of generated charge carriers) of an anisotropic RGO-hybridized polymer film observed along the orthogonal (red) and parallel (blue) directions to the film surface, upon laser excitation at 355 nm (photon density, 9.1 × 10^{15} photons cm^{-2}) with a pulse duration of 5−8 ns at 25 °C. Inset: Time-resolved decay profiles of the photogenerated charge carriers.

electroconductivity by using the flash-photolysis time-resolved microwave conductivity (FP-TRMC) measurement, which allows for evaluating intrinsic carrier transport properties of materials without electrodes.[64,65] Since the FP-TRMC technique is not applicable to samples containing dielectric solvents, the RGO-hybridized hydrogel film was converted into a water-free polymeric material by the replacement of internal water with an acrylamide monomer (*N*,*N*-dimethylacrylamide) and subsequent polymerization of the monomer. The resultant polymer film was placed in a microwave cavity in such a way that the electric-field vector (*E*) of the microwave can be polarized orthogonal or parallel to the film surface. Upon laser flash, the film displayed rise and decay profiles of the transient conductivity, given by $\phi\Sigma\mu$ (Figure 8, inset), where ϕ and $\Sigma\mu$ represent photocarrier generation yield and sum of the mobilities of generated charge carriers, respectively. From the FP-TRMC profiles, the maximum transient conductivities ($\phi\Sigma\mu_{max}$) of the film along the orthogonal (Figure 8, red) and parallel (blue) directions to the film surface were evaluated as 2.2 × 10^{-4} and 1.3 × 10^{-4} cm^2 V^{-1} s^{-1}, respectively. Worth noting is that a meaningful degree of anisotropy (~1.7) was observed for the electroconductivity of the RGO-hybridized hydrogel film, even though the amount of RGO was less than 0.5 wt %.

CONCLUSIONS

Under a magnetic field (5−10 T), the aqueous dispersions of graphene oxide (GO, 0.02−0.2 wt %) were successfully converted into composite hydrogels containing anisotropically oriented GO, using an *in situ* polymerization process involving an acryl monomer and a cross-linker. Unlike the conventional methods used for the preparation of composite materials with anisotropically oriented GO, the present method can orient intact GO with essentially no limitation in orientation direction and sample shape.

From the viewpoint of fundamental science, hydrogels developed here will serve as useful samples for the study of the magnetic orientation of GO. Through the systematic investigation of the hydrogels using 2D SAXS, the following insights were gleaned. (i) GO planes are oriented parallel to the applied magnetic

field. (ii) Under optimal conditions, excellent orientation can be achieved (orientation order parameter = 0.80). (iii) Effects of magnetic-field intensity, GO concentration, and GO size on the orientational order are clarified. (iv) The present method is applicable over an unprecedentedly wide range of GO concentrations (0.02−0.2 wt %).

For practical applications, our composite hydrogels underwent the following conversions without a drastic deterioration in the gel network and oriented structure of GO: (i) GO in the hydrogel was readily converted into RGO by treatment with reductants; (ii) internal water of the hydrogels hybridized with anisotropically oriented GO/RGO was replaced with organic solvents and an ionic liquid to afford organogels and ionogels, respectively. Given the easy preparation, generality in terms of sample shape and GO concentration, and excellent orientation order, the present GO/RGO-hybridized hydrogels could potentially serve as novel carbon-based soft materials.

EXPERIMENTAL METHODS

Materials. Expandable graphite (GRAFGuard 160-50N, averaged size = ~350 μm) was given by TOMOE Engineering Co., Ltd. Synthetic graphite powder (SGO-45, averaged size = ~45 μm) was purchased from SEC Carbon, Ltd. All chemicals were used as received.

General Procedures. Raman spectra were recorded using a Jobin-Yvon model LabRAM H-800 spectrometer equipped with a 514 nm Ar-ion laser as the excitation source. Infrared (IR) spectra were recorded at 25 °C on a JASCO model FT/IR-4100 Fourier transform infrared spectrometer. Atomic force microscopy was performed by a JEOL JSPM-5200 scanning probe microscope under tapping mode (phase imaging). Scanning electron microscopy with energy dispersion X-ray spectrometry (SEM/EDS) was carried out on a JEOL JSM-6330F/JED-2200. A JASTEC JMTD-10T100 superconducting magnet with a vertical bore of 100 mm was used for the preparation of hydrogels with magnetically oriented GO nanosheets. Polarized optical microscopy was performed under crossed polarizers by using a Nikon model Eclipse LV100POL optical polarizing microscope. Rheological tests of hydrogels were carried out at 25 °C by using an Anton Paar model MCR-301 rheometer, with a 25 mm diameter parallel plate attached to a transducer. The gap was set at 5 mm. X-ray photoelectron spectroscopy was carried out using a Thermo Fischer Scientific KK model ESCALAB 250 spectrometer.

Preparation of Graphene Oxide Samples. For the preparation of a GO sample with larger average size (~50 μm), expandable graphite (average size = ~350 μm) was pretreated with a microwave and then oxidized and exfoliated by using a modification of Hummers's method.[52,53] Briefly, concentrated H_2SO_4 (138 mL), $NaNO_3$ (3.0 g), and $KMnO_4$ (18.0 g) were successively added to graphite (3.0 g) at 0 °C. After being allowed to warm to 35 °C, the mixture was treated with water (240 mL), heated to 90 °C, and then treated with 30% H_2O_2 (9.0 mL) to afford a suspension of a yellow paste. The solid mass was collected by ultrahigh-speed centrifugation (1×10^4 rpm) and successively washed with aqueous HCl (30%, 3×100 mL) and deionized water (100 mL). The resultant solid was dried in air to afford GO as a black powder (2.8 g). A GO sample with smaller average size (~0.3 μm) was prepared from the synthetic graphite powder sample with an average size of 45 μm (SGO-45), by using the modification of Hummers's method[52] as above. Characterizations of the resultant GO samples are given in the Supporting Information (Figures S1−S4).

Preparation of GO-Hybridized Hydrogels. Typically, an aqueous GO dispersion was prepared by sonication of a mixture of water and GO powder (average size = ~50 μm; 0.20 wt %).[31,52,53] To the aqueous GO suspension (6.0 mL) were added an acryl monomer (*N*,*N*-dimethylacrylamide, 200 mg) and a cross-linker (*N*,*N*′-methylenebis(acrylamide), 10 mg) and dissolved. The mixture was left to stand in the bore of a superconducting magnet (10 T) at 20 °C for 30 min and then successively treated with an aqueous solution of potassium persulfate (50 mg mL^{-1}, 20 μL) and *N*,*N*,*N*′,*N*′-tetramethylethylenediamine (10 μL). The resultant mixture was allowed to stand at 20 °C in the 10 T magnetic field for 12 h to afford a GO-hybridized hydrogel.

2D Small-Angle X-ray Scattering Measurement. 2D SAXS was carried out at BL45XU in SPring-8 (Hyogo, Japan)[66] with a Rigaku imaging plate area detector model R-AXIS IV++. The scattering vector q [$q = 4\pi \sin\theta/\lambda$; 2θ and λ are scattering angle and wavelength of the incident X-ray beam (1.00 Å), respectively] and the position of an incident X-ray beam on the detector were calibrated using several orders of layer reflections from silver behenate (d = 58.380 Å). The sample-to-detector distance was 2.5 m. A hydrogel sample was sliced into films with a thickness of ~1 mm just before SAXS measurements. For azimuthal angle (see Figure 2, φ) plots, scattering in 2D SAXS images at q = 0.08−0.44 nm^{-1} was integrated for every 5° in azimuthal angle, by using Rigaku model R-AXIS Display software.

Chemical Reduction of GO to RGO in the Anisotropic Hydrogel (refs 59, 60). A GO-hybridized hydrogel (~50 μm-sized GO/monomer/cross-linker = 0.20/3.0/0.16 wt %, 1.0 g) was immersed in an aqueous solution (10 mL) of KOH (1.6 M) at 20 °C for 2 h and then in an aqueous solution (10 mL) of HI (55%) at 20 °C for 12 h. Then, in order to remove excess chemicals, the resultant material was soaked in fresh water (20 mL) twice for 12 h at 20 °C.

Conversion of GO/RGO-Hybridized Hydrogels into Organo- and Ionogels. A GO-hybridized hydrogel (~50 μm-sized GO/monomer/cross-linker = 0.20/3.0/0.16 wt %, 1.0 g) was immersed in 10 mL of a fresh solvent (EtOH, EG, or $BMImBF_4$) three times for 12 h at 20 °C. Likewise, an RGO-hybridized hydrogel, prepared by the chemical reduction of GO in the GO-hybridized hydrogel, was converted into the organo- and ionogels.

Preparation of an RGO-Hybridized Polymer Film. A film-shaped GO-hybridized hydrogel film (1 mm thick, 10 mm × 20 mm width, ~50 μm-sized GO/monomer/cross-linker = 0.20/3.0/0.16 wt %) was prepared in a 10 T magnetic field that was directed orthogonal to the film surface. The resultant GO-hybridized hydrogel film was subjected to the chemical reduction as described above to afford an RGO-hybridized hydrogel film (~1 mm thick). The RGO-hybridized hydrogel film was immersed in *N*,*N*-dimethylacrylamide (10 mL) containing 2,2-diethoxyacetophenone (1 wt %) at 20 °C for 12 h three times in a fresh mixture of *N*,*N*-dimethylacrylamide and 2,2-diethoxyacetophenone. The gel film was exposed to a 500 W high-pressure mercury arc light (>360 nm) at 20 °C for 30 min, whereupon radical polymerization of *N*,*N*-dimethylacrylamide proceeded. The resultant polymer film was extensively washed with acetone and then air-dried.

Flash-Photolysis Time-Resolved Microwave Conductivity Measurements. FP-TRMC measurements were carried out at 25 °C in air, where the resonant frequency and microwave power were properly adjusted to 9.1 GHz and 10 mW, respectively. The RGO-hybridized polymer film was placed on a quartz substrate. Charge carriers were photochemically generated upon exposure to a 355 nm laser pulse from a Spectra Physics model INDI-HG Nd:YAG laser with a pulse duration of 5−8 ns. The photon density was 9.1×10^{15} photons cm^{-2}. The $\varphi\Sigma\mu$ value was evaluated according to $\varphi\Sigma\mu = \Delta\sigma/(eF_{light}I_0)$, where φ, $\Sigma\mu$, e, F_{light}, I_0, and $\Delta\sigma$ represent charge carrier generation yield, sum of charge carrier mobilities, elementary charge, correction factor, photon density of incident laser pulse, and transient photoconductivity, respectively.

Conflict of Interest: The authors declare no competing financial interest.

Acknowledgment. This work was also supported by a Grant-in-Aid for Specially Promoted Research (25000005) on "Physically Perturbed Assembly for Tailoring High-Performance Soft Materials with Controlled Macroscopic Structural Anisotropy". The synchrotron X-ray diffraction experiments were performed at BL45XU at SPring-8 with approval of the RIKEN SPring-8 Center (proposal 20120051). We are grateful to T. Hikima and M. Yamamoto for their assistance in data collection at BL45XU at SPring-8. We also thank D. Hashizume and D. Inoue for SEM/EDS measurements.

Supporting Information Available: Details regarding the estimation of the orientation order parameter and characterization of GO and GO/RGO-hybridized hydrogels. This material is available free of charge *via* the Internet at http://pubs.acs.org.

REFERENCES AND NOTES

1. Jacobson, A. J. Colloidal Dispersions of Compounds with Layer and Chain Structures. *Mater. Sci. Forum* **1994**, *152−153*, 1–12.
2. Jacobson, A. J. In *Comprehensive Supramolecular Chemistry*, Vol. 7; Alberti, G.; Bein, T., Eds.; Elsevier Science: Oxford, U.K., 1996; pp 315−335.
3. Novoselov, K. S.; Jiang, D.; Schedin, F.; Booth, T. J.; Khotkevich, V. V.; Morozov, S. V.; Geim, A. K. Two-Dimensional Atomic Crystals. *Proc. Natl. Acad. Sci. U.S.A.* **2005**, *102*, 10451–10453.
4. Sakamoto, J.; van Heijst, J.; Lukin, O.; Schlüter, A. D. Two-Dimensional Polymers: Just a Dream of Synthetic Chemists? *Angew. Chem., Int. Ed.* **2009**, *48*, 1030–1069.
5. Ma, R.; Sasaki, T. Nanosheets of Oxides and Hydroxides: Ultimate 2D Charge-Bearing Functional Crystallites. *Adv. Mater.* **2010**, *22*, 5082–5104.
6. Dikin, D. A.; Stankovich, S.; Zimney, E. J.; Piner, R. D.; Dommett, G. H. B.; Evmenenko, G.; Nguyen, S. T.; Ruoff, R. S. Preparation and Characterization of Graphene Oxide Paper. *Nature* **2007**, *448*, 457–460.
7. Li, D.; Müller, M. B.; Gilje, S.; Kaner, R. B.; Wallace, G. G. Processable Aqueous Dispersions of Graphene Nanosheets. *Nat. Nanotechnol.* **2008**, *3*, 101–105.
8. Gómez-Navarro, C.; Burghard, M.; Kern, K. Elastic Properties of Chemically Derived Single Graphene Sheets. *Nano Lett.* **2008**, *8*, 2045–2049.
9. Segal, M. Selling Graphene by the Ton. *Nat. Nanotechnol.* **2009**, *4*, 612–614.
10. Geim, A. K. Graphene: Status and Prospects. *Science* **2009**, *324*, 1530–1534.
11. Dreyer, D. R.; Park, S.; Bielawski, C. W.; Ruoff, R. S. The Chemistry of Graphene Oxide. *Chem. Soc. Rev.* **2010**, *39*, 228–240.
12. He, H. K.; Gao, C. General Approach to Individually Dispersed, Highly Soluble, and Conductive Graphene Nanosheets Functionalized by Nitrene Chemistry. *Chem. Mater.* **2010**, *22*, 5054–5064.
13. Zhu, Y.; Murali, S.; Cai, W.; Li, X.; Suk, J. W.; Potts, J. R.; Ruoff, R. S. Graphene and Graphene Oxide: Synthesis, Properties, and Applications. *Adv. Mater.* **2010**, *22*, 3906–3924.
14. Nair, R. R.; Wu, H. A.; Jayaram, P. N.; Grigorieva, I. V.; Geim, A. K. Unimpeded Permeation of Water through Helium-Leak−Tight Graphene-Based Membranes. *Science* **2012**, *335*, 442–444.
15. Stankovich, S.; Dikin, D. A.; Piner, R. D.; Kohlhaas, K. A.; Kleinhammes, A.; Jia, Y.; Wu, Y.; Nguyen, S. T.; Ruoff, R. S. Synthesis of Graphene-Based Nanosheets *via* Chemical Reduction of Exfoliated Graphite Oxide. *Carbon* **2007**, *45*, 1558–1565.
16. Gao, W.; Alemany, L. B.; Ci, L.; Ajayan, P. M. New Insights into the Structure and Reduction of Graphite Oxide. *Nat. Chem.* **2009**, *1*, 403–408.
17. Compton, O. C.; Nguyen, S. T. Graphene-Based Materials: Synthesis, Characterization, Properties, and Applications. *Small* **2011**, *7*, 1876–1902.
18. Pei, S.; Cheng, H. M. The Reduction of Graphene Oxide. *Carbon* **2012**, *50*, 3210–3228.
19. Goncalves, G.; Marques, P. A. A. P.; Barros-Timmons, A.; Bdkin, I.; Singh, M. K.; Emami, N.; Gracio, J. Graphene Oxide Modified with PMMA *via* ATRP as a Reinforcement Filler. *J. Mater. Chem.* **2010**, *20*, 9927–9934.
20. Sengupta, R.; Bhattacharya, M.; Bandyopadhyay, S.; Bhowmick, A. K. A Review on the Mechanical and Electrical Properties of Graphite and Modified Graphite Reinforced Polymer Composites. *Prog. Polym. Sci.* **2011**, *36*, 638–670.
21. Alzari, V.; Nuvoli, D.; Scognamillo, S.; Piccinini, M.; Gioffredi, E.; Malucelli, G.; Marceddu, S.; Sechi, M.; Sanna, V.; Mariani, A. Graphene-Containing Thermoresponsive Nanocomposite Hydrogels of Poly(*N*-isopropylacrylamide) Prepared by Frontal Polymerization. *J. Mater. Chem.* **2011**, *21*, 8727–8733.
22. Zhu, C. H.; Lu, Y.; Peng, J.; Chen, J. F.; Yu, S. H. Photothermally Sensitive Poly(*N*-isopropylacrylamide)/Graphene Oxide Nanocomposite Hydrogels as Remote Light-Controlled Liquid Microvalves. *Adv. Funct. Mater.* **2012**, *22*, 4017–4022.
23. Liu, R.; Liang, S.; Tang, X.-Z.; Yan, D.; Li, X.; Yu, Z.-Z. Tough and Highly Stretchable Graphene Oxide/Polyacrylamide Nanocomposite Hydrogels. *J. Mater. Chem.* **2012**, *22*, 14160–14167.
24. Podsiadlo, P.; Kaushik, A. K.; Arruda, E. M.; Waas, A. M.; Shim, B. S.; Xu, J.; Nandivada, H.; Pumplin, B. G.; Lahann, J.; Ramamoorthy, A.; *et al.* Ultrastrong and Stiff Layered Polymer Nanocomposites. *Science* **2007**, *318*, 80–83.
25. Kobayashi, Y.; Schottenfeld, J. A.; Macdonald, D. D.; Mallouk, T. E. Structural Effects in the Protonic/Electronic Conductivity of Dion-Jacobson Phase Niobate and Tantalate Layered Perovskites. *J. Phys. Chem. C* **2007**, *111*, 3185–3191.
26. Bonderer, L. J.; Studart, A. R.; Gauckler, L. J. Bioinspired Design and Assembly of Platelet Reinforced Polymer Films. *Science* **2008**, *319*, 1069–1073.
27. Veca, L. M.; Meziani, M. J.; Wang, W.; Wang, X.; Lu, F.; Zhang, P.; Lin, Y.; Fee, R.; Connell, J. W.; Sun, Y.-P. Carbon Nanosheets for Polymeric Nanocomposites with High Thermal Conductivity. *Adv. Mater.* **2009**, *21*, 2088–2092.
28. Haque, M. A.; Kamita, G.; Kurokawa, T.; Tsujii, K.; Gong, J. P. Unidirectional Alignment of Lamellar Bilayer in Hydrogel: One-Dimensional Swelling, Anisotropic Modulus, and Stress/Strain Tunable Structural Color. *Adv. Mater.* **2010**, *22*, 5110–5114.
29. Cardinali, M.; Valentini, L.; Kenny, J. M. Anisotropic Electrical Transport Properties of Graphene Nanoplatelets/Pyrene Composites by Electric-Field-Assisted Thermal Annealing. *J. Phys. Chem. C* **2011**, *115*, 16652–16656.
30. Erb, R. M.; Libanori, R.; Rothfuchs, N.; Studart, A. R. Composites Reinforced in Three Dimensions by Using Low Magnetic Fields. *Science* **2012**, *335*, 199–204.
31. Cote, L. J.; Kim, F.; Huang, J. X. Langmuir−Blodgett Assembly of Graphite Oxide Single Layers. *J. Am. Chem. Soc.* **2009**, *131*, 1043–1049.
32. Zheng, Q. B.; Ip, W. H.; Lin, X.; Yousefi, N.; Yeung, K. K.; Li, Z.; Kim, J. K. Transparent Conductive Films Consisting of Ultralarge Graphene Sheets Produced by Langmuir−Blodgett Assembly. *ACS Nano* **2011**, *5*, 6039–6051.
33. Chen, H.; Muller, M. B.; Gilmore, K. J.; Wallace, G. G.; Li, D. Mechanically Strong, Electrically Conductive, and Biocompatible Graphene Paper. *Adv. Mater.* **2008**, *20*, 3557–3561.
34. Xu, Y.; Hong, W.; Bai, H.; Li, C.; Shi, G. Strong and Ductile Poly(vinyl alcohol)/Graphene Oxide Composite Films with a Layered Structure. *Carbon* **2009**, *47*, 3538–3543.
35. Wu, Q.; Xu, Y.; Yao, Z.; Liu, A.; Shi, G. Supercapacitors Based on Flexible Graphene/Polyaniline Nanofiber Composite Films. *ACS Nano* **2010**, *4*, 1963–1970.
36. Putz, K. W.; Compton, O. C.; Palmeri, M. J.; Nguyen, S. T.; Brinson, L. C. High-Nanofiller-Content Graphene Oxide−Polymer Nanocomposites *via* Vacuum-Assisted Self-Assembly. *Adv. Funct. Mater.* **2010**, *20*, 3322–3329.
37. Putz, K. W.; Compton, O. C.; Segar, C.; An, Z.; Nguyen, S. B. T.; Brinson, L. C. Evolution of Order During Vacuum-Assisted Self-Assembly of Graphene Oxide Paper and Associated Polymer Nanocomposites. *ACS Nano* **2011**, *5*, 6601–6609.

38. Lin, X.; Shen, X.; Zheng, Q.; Yousefi, N.; Ye, L.; Mai, Y.-W.; Kim, J.-K. Fabrication of Highly-Aligned, Conductive, and Strong Graphene Papers Using Ultralarge Graphene Oxide Sheets. *ACS Nano* **2012**, *6*, 10708–10719.
39. Youn, S. C.; Kim, D. W.; Yang, S. B.; Cho, H. M.; Lee, J. H.; Jung, H.-T. Vertical Alignment of Reduced Graphene Oxide/Fe-Oxide Hybrids Using the Magneto-Evaporation Method. *Chem. Commun.* **2011**, *47*, 5211–5213.
40. Eguchi, M.; Angelone, M. S.; Yennawar, H. P.; Mallouk, T. E. Anisotropic Alignment of Lamellar Potassium Hexaniobate Microcrystals and Nanoscrolls in a Static Magnetic Field. *J. Phys. Chem. C* **2008**, *112*, 11280–11285.
41. van der Beek, D.; Petukhov, A. V.; Davidson, P.; Ferré, J.; Jamet, J. P.; Wensink, H. H.; Vroege, G. J.; Bras, W.; Lekkerkerker, H. N. W. Magnetic-Field-Induced Orientational Order in the Isotropic Phase of Hard Colloidal Platelets. *Phys. Rev. E* **2006**, *73*, 041402-1–041402-10.
42. Loudet-Courreges, C.; Nallet, F.; Dufourc, E. J.; Oda, R. Unprecedented Observation of Days-Long Remnant Orientation of Phospholipid Bicelles: A Small-Angle X-Ray Scattering and Theoretical Study. *Langmuir* **2011**, *27*, 9122–9130.
43. Kaneko, Y.; Shimada, S.; Fukuda, T.; Kimura, T.; Yokoi, H.; Matsuda, H.; Onodera, T.; Kasai, H.; Okada, S.; Oikawa, H.; *et al*. A Novel Method for Fixing the Anisotropic Orientation of Dispersed Organic Nanocrystals in a Magnetic Field. *Adv. Mater.* **2005**, *17*, 160–163.
44. Torbet, J.; Maret, G. Fibres of Highly Oriented Pf1 Bacteriophage Produced in a Strong Magnetic Field. *J. Mol. Biol.* **1979**, *134*, 843–845.
45. Stamenov, P.; Coey, J. M. D. Magnetic Susceptibility of Carbon — Experiment and Theory. *J. Magn. Magn. Mater.* **2005**, *290—291*, 279–285.
46. Pauling, L. The Diamagnetic Anisotropy of Aromatic Molecules. *J. Chem. Phys.* **1936**, *4*, 673–677.
47. Kim, J. E.; Han, T. H.; Lee, S. H.; Kim, J. Y.; Ahn, C. W.; Yun, J. M.; Kim, S. O. Graphene Oxide Liquid Crystals. *Angew. Chem., Int. Ed.* **2011**, *50*, 3043–3047.
48. Torbet, J.; Freyssinet, J. M.; Hudry-Clergeon, G. Oriented Fibrin Gels Formed by Polymerization in Strong Magnetic Fields. *Nature* **1981**, *289*, 91–93.
49. Momota, H.; Yokoi, H.; Takamasu, T. Development of Magnetically Aligned Single-Walled Carbon Nanotubes—Gelatin Composite Films. *J. Nanosci. Nanotechnol.* **2010**, *10*, 3849–3853.
50. Sklute, E. C.; Eguchi, M.; Henderson, C. N.; Angelone, M. S.; Yennawar, H. P.; Mallouk, T. E. Orientation of Diamagnetic Layered Transition Metal Oxide Particles in 1-T Magnetic Fields. *J. Am. Chem. Soc.* **2011**, *133*, 1824–1831.
51. Maggini, L.; Liu, M.; Ishida, Y.; Bonifazi, D. Anisotropically Luminescent Hydrogels Containing Magnetically-Aligned MWCNTs-Eu(III) Hybrids. *Adv. Mater.* **2013**, *25*, 2462–2467.
52. Hummers, W. S.; Offeman, R. E. Preparation of Graphitic Oxide. *J. Am. Chem. Soc.* **1958**, *80*, 1339–1339.
53. Luo, Z.; Lu, Y.; Somers, L. A.; Johnson, A. T. C. High Yield Preparation of Macroscopic Graphene Oxide Membranes. *J. Am. Chem. Soc.* **2009**, *131*, 898–899.
54. Qazi, S. J. S.; Rennie, A. R.; Wright, J. P.; Cockcroft, J. K. Alignment of Plate-Like Particles in a Colloidal Dispersion under Flow in a Uniform Pipe Studied by High-Energy X-Ray Diffraction. *Langmuir* **2010**, *26*, 18701–18709.
55. Feng, S.; Xiong, X.; Zhang, G.; Xia, N.; Chen, Y.; Wang, W. Hierarchical Structure in Oriented Fibers of a Dendronized Polymer. *Macromolecules* **2009**, *42*, 281–287.
56. Nie, Y. J.; Huang, G. S.; Qu, L. L.; Wang, X.; Weng, G. S.; Wu, J. R. New Insights into Thermodynamic Description of Strain-Induced Crystallization of Peroxide Cross-Linked Natural Rubber Filled with Clay by Tube Model. *Polymer* **2011**, *52*, 3234–3242. For the evaluation of the orientation order parameter, see also the Supporting Information (Section 1).
57. Xu, Z.; Gao, C. Aqueous Liquid Crystals of Graphene Oxide. *ACS Nano* **2011**, *5*, 2908–2915.
58. Dan, B.; Behabtu, N.; Martinez, A.; Evans, J. S.; Kosynkin, D. V.; Tour, J. M.; Pasquali, M.; Smalyukh, I. I. Liquid Crystals of Aqueous, Giant Graphene Oxide Fakes. *Soft Matter* **2011**, *7*, 11154–11159.
59. Park, S.; An, J.; Piner, R. D.; Jung, I.; Yang, D.; Velamakanni, A.; Nguyen, S. B. T.; Ruoff, R. S. Aqueous Suspension and Characterization of Chemically Modified Graphene Sheets. *Chem. Mater.* **2008**, *20*, 6592–6594.
60. Pei, S.; Zhao, J.; Du, J.; Ren, W.; Cheng, H. M. Direct Reduction of Graphene Oxide Films into Highly Conductive and Flexible Graphene Films by Hydrohalic Acids. *Carbon* **2010**, *48*, 4466–4474.
61. Becerril, H. A.; Mao, J.; Liu, Z.; Stoltenberg, R. M.; Bao, Z.; Chen, Y. Evaluation of Solution-Processed Reduced Graphene Oxide Films as Transparent Conductors. *ACS Nano* **2008**, *2*, 463–470.
62. Wu, Y. H.; Yang, B. Effects of Localized Electric Field on the Growth of Carbon Nanowalls. *Nano Lett.* **2002**, *2*, 355–359.
63. Liang, Q.; Yao, X.; Wang, W.; Liu, Y.; Wong, C. P. A Three-Dimensional Vertically Aligned Functionalized Multilayer Graphene Architecture: An Approach for Graphene-Based Thermal Interfacial Materials. *ACS Nano* **2011**, *5*, 2392–2401.
64. Saeki, A.; Seki, S.; Takenobu, T.; Iwasa, Y.; Tagawa, S. Mobility and Dynamics of Charge Carriers in Rubrene Single Crystals Studied by Flash-Photolysis Microwave Conductivity and Optical Spectroscopy. *Adv. Mater.* **2008**, *20*, 920–923.
65. Babu, S. S.; Saeki, A.; Seki, S.; Möhwald, H.; Nakanishi, T. Millimeter-Sized Flat Crystalline Sheet Architectures of Fullerene Assemblies with Anisotropic Photoconductivity. *Phys. Chem. Chem. Phys.* **2011**, *13*, 4830–4834.
66. Fujisawa, T.; Inoue, K.; Oka, T.; Iwamoto, H.; Uruga, T.; Kumasaka, T.; Inoko, Y.; Yagi, N.; Yamamoto, M.; Ueki, T. Small-Angle X-Ray Scattering Station at the SPring-8 RIKEN Beamline. *J. Appl. Crystallogr.* **2000**, *33*, 797–800.